Dynamic Changes in Pancreatic Endocrine Cell Abundance, Distribution, and Function in Antigen-Induced and Spontaneous Autoimmune Diabetes

Klaus Pechhold,[1] Xiaolong Zhu,[1] Victor S. Harrison,[1] Janet Lee,[1] Sagarika Chakrabarty,[1] Kerstin Koczwara,[1,2] Oksana Gavrilova,[3] and David M. Harlan[1]

OBJECTIVE—Insulin deficiency in type 1 diabetes and in rodent autoimmune diabetes models is caused by β-cell–specific killing by autoreactive T-cells. Less is known about β-cell numbers and phenotype remaining at diabetes onset and the fate of other pancreatic endocrine cellular constituents.

RESEARCH DESIGN AND METHODS—We applied multicolor flow cytometry, confocal microscopy, and immunohistochemistry, supported by quantitative RT-PCR, to simultaneously track pancreatic endocrine cell frequencies and phenotypes during a T-cell–mediated β-cell–destructive process using two independent autoimmune diabetes models, an inducible autoantigen-specific model and the spontaneously diabetic NOD mouse.

RESULTS—The proportion of pancreatic insulin-positive β-cells to glucagon-positive α-cells was about 4:1 in nondiabetic mice. Islets isolated from newly diabetic mice exhibited the expected severe β-cell depletion accompanied by phenotypic β-cell changes (i.e., hypertrophy and degranulation), but they also revealed a substantial loss of α-cells, which was further confirmed by quantitative immunohistochemisty. While maintaining normal randomly timed serum glucagon levels, newly diabetic mice displayed an impaired glucagon secretory response to non–insulin-induced hypoglycemia.

CONCLUSIONS—Systematically applying multicolor flow cytometry and immunohistochemistry to track declining β-cell numbers in recently diabetic mice revealed an altered endocrine cell composition that is consistent with a prominent and unexpected islet α-cell loss. These alterations were observed in induced and spontaneous autoimmune diabetes models, became apparent at diabetes onset, and differed markedly within islets compared with sub–islet-sized endocrine cell clusters and among pancreatic lobes. We propose that these changes are adaptive in nature, possibly fueled by worsening glycemia and regenerative processes. ***Diabetes*** **58:1175–1184, 2009**

From the [1]Diabetes Branch, National Institute of Diabetes and Digestive and Kidney Diseases, National Institutes of Health, Bethesda, Maryland; the [2]Institute for Diabetes Research, Research Group for Diabetes at the Helmholtz Center, Munich, Germany; and the [3]Mouse Metabolism Core, National Institute of Diabetes and Digestive and Kidney Diseases, National Institutes of Health, Bethesda, Maryland.

Corresponding author: Klaus Pechhold, klausp@intra.niddk.nih.gov.

Received 27 October 2007 and accepted 13 February 2009.

Published ahead of print at http://diabetes.diabetesjournals.org on 19 February 2009. DOI: 10.2337/db08-0616.

S.C. is currently affiliated with The National Eye Institute of the National Institutes of Health, Bethesda, Maryland.

Although much has been learned about β-cell development and β-cell biology and function in vitro (using isolated pancreatic islets), studies designed to examine β-cell phenotype in vivo have suffered from technical limitations. For instance, currently available techniques to quantify pancreatic β-cell mass rely on laborious histomorphometric techniques (1) or on assumptions that β-cell mass correlates with β-cell function (stimulated C-peptide release) (2) or total pancreatic insulin content (3,4). Furthermore, quantifying the different endocrine islet cellular constituents by staining for the hormones produced (i.e., glucagon by α-cells, insulin by β-cells, somatostatin by δ-cells, and pancreatic polypeptide by PP-cells) has to date been challenging, relying again mostly on histomorphometry, and automated image processing setups typically allow only single-parameter analysis (5,6).

Although preparative fluorescence-activated cell sorting of islet β-cells has been attempted (7–10), wider application has been limited by the lack of islet endocrine cell surface markers and insufficient resolution by autofluorescence, especially in species other than rats (11). Fluorescence reagents with islet granule affinity to identify β-cells in both mice (12) and humans (13) have limited utility, presumably because β-cells are degranulated by hyperglycemia. Other methods, such as quantitative (q)RT-PCR and analytical multicolor/multiparameter flow cytometry, capable of precise phenotypic and functional assessment, have been hampered by both the notorious difficulty to reliably prepare pancreatic RNA (14) and the fact that the pancreas is a heterogeneous organ comprised of irregularly intermixed exocrine and endocrine tissues. Even so-called "purified" isolated pancreatic islets from naïve mice (or other mammals) represent a multitude of specialized cell types (15), which is further complicated in animals with autoimmune diabetes when abundant inflammatory cells invade the islets (16).

Recognizing these limitations, we adapted flow cytometry techniques for pancreatic studies and, together with qRT-PCR, confocal immunofluorescence microscopy, and quantitative immunohistochemistry, characterized the pancreatic endocrine islet cell components in naïve and recently diabetic mice. We now report that pancreatic islets isolated from mice developing T-cell–mediated β-cell–specific autoimmune diabetes demonstrate an unexpected glucagon-positive α-cell loss roughly commensurate with the expected β-cell loss.

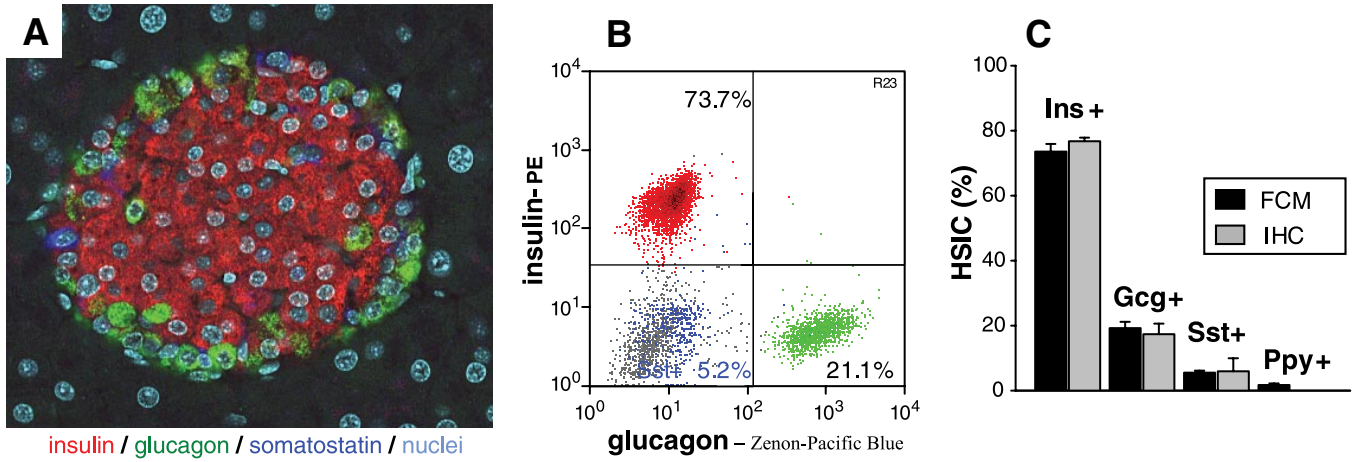

FIG. 1. Pancreatic islet hormone-secreting cell subsets as assessed by immunofluorescence and flow cytometry. *A*: Pancreas section from a naïve C57BL/6 mouse simultaneously stained for the three major endocrine cell subsets: insulin positive (β-cells, red), glucagon positive (α-cells, green), and somatostatin positive (δ-cells, dark blue). Nuclei are shown in turquoise. Magnification ×400. *B*: Islet endocrine cells by flow cytometry. Handpicked pancreatic islets isolated from one naïve C57BL/6 mouse were dissociated into a single-cell suspension and intracytoplasmically stained for insulin (red), glucagon (green), and somatostatin (blue). All other islet components (e.g., other endocrine, endothelial cells) and residual exocrine cells are depicted in gray. For presentation purposes, insulin-, glucagon-, and somatostatin-positive endocrine cell subsets (typically making up ~80% of healthy islets) were normalized to 100%. *C*: Quantitative analysis of islet cell subsets of naïve C57BL/6 mice by flow cytometry (■) and immunofluorescence (▨). For flow cytometry, >10,000 events of dissociated and stained islet cells per mouse were acquired. Frequencies (means ± SE, $n = 5$ mice) were: insulin positive 73.5 ± 2.4%, glucagon positive 19.2 ± 1.9%, somatostatin positive 5.5 ± 0.6%, and pancreatic polypeptide positive 1.7 ± 0.5%. For immunofluorescence, the three major endocrine cell subsets were quantified by independent, triplicate, or quadruplicate scorings (>350 endocrine cells were counted of at least 12 randomly selected islets). Their frequencies (means ± SE, $n = 3$ mice) were 76.7 ± 1.1%, 17.3 ± 3.3%, and 5.9 ± 4.0% for insulin-, glucagon-, and somatostatin-positive cells, respectively. Gcg, glucagon; Ins, insulin; Ppy, pancreatic polypeptide; Sst, somatostatin. (A high-quality digital representation of this figure is available in the online issue.)

RESEARCH DESIGN AND METHODS

Rat insulin promoter (Rip) lymphocytic choriomeningitis virus (LCMV)-glycoprotein (GP) × Rip-CD80 bitransgenic mice (17), NOD mice, and fully backcrossed NOD-Rag1 null or NOD-SCID mice (both from Jackson Labs) were used as autoimmune diabetes models and controls, respectively. GP-specific, T-cell receptor–(TCR) transgenic mice—p14 strain (18), Rag1 null—were used as a source of monoclonal, β-cell–specific $CD8^+$ T-cells. All mice were housed at the Division of Veterinary Resources, National Institutes of Health, in accordance with the guidelines set forth by the committee on the care and use of laboratory animals on a protocol approved by the animal care and use committee of the National Institute of Diabetes and Digestive and Kidney Diseases.

$CD8^+$ T-cell purification and in vitro T-cell activation. TCR-transgenic $CD8^+$ T-cells (P14 strain, Rag1 null) were purified by immunodepleting spleen and lymph node cells expressing I-A^b, CD11b, and NK1.1, yielding cells that were 86–95% $CD8^+$ T-cells. These cells ($0.5 \times 10^6/cm^2$) were stimulated for 3–4 days in the presence of γ-interferon–pretreated fibroblasts incubated with the GP agonist peptide (LCMV-GP amino acids 33–41 at 0.1 μmol/l for 1 h). Cultures were supplemented with interleukin-2 (2 ng/ml) after 48 h. On day 3 of culture, >98% of viable cells were $CD8^+$ TCR-transgenic by flow cytometry (data not shown).

Diabetes induction and diagnosis. We have studied a transgenic mouse model of immune-mediated β-cell destruction and diabetes that relies on the mouse β-cells expressing the LCMV GP under the control of Rip. If such mice are infected with LCMV, the antiviral immune response also leads to fulminant diabetes. We have modified that system by creating bitransgenic mice such that their β-cells also specifically express the T-cell costimulatory ligand CD80 (4). These mice are highly susceptible to autoimmune β-cell destruction induced by immunizing with the GP antigen, a model system we've named experimental autoimmune diabetes (EAD) (17). For these studies, we adoptively transferred in vitro activated LCMV-GP–specific cytotoxic T-lymphocytes (CTLs; 10^6 per mouse) to the Rip-$CD80^+GP^+$ recipients. This EAD system initiates a slowly progressive anti–β-cell–specific immune destructive process such that diabetes develops 53 ± 9 days after CTL transfer. At ~4 weeks after CTL transfer, nondiabetic mice were checked daily for diabetes development, indicated by glycosuria and confirmed when blood glucose readings were >14 mmol/l.

Islet isolation and islet cell flow cytometry. Pancreatic islets were isolated by standard techniques. Briefly, pancreata were inflated via bile duct cannulation and retrograde pancreatic duct injection of 3–4 ml of ice-cold collagenase type V (1 mg/ml in Hank's balanced salt solution). After digestion (37°C, 14 min), pancreata were dispersed by aspirating through a 14-G needle, filtered through a metal strainer (0.8 mm), and subjected to buoyant density gradient centrifugation (14–15% Optiprep; Accurate Chemicals, Westbury, NY). After islets were carefully picked, the remaining viable pancreatic cells were also collected. These cells containing sub–islet-sized endocrine clusters and single endocrine cells were termed islet-depleted cells.

Isolated islets (and islet-depleted cells) were dissociated into a single-cell suspension by gentle pipetting after washing in 2 mmol/l EDTA/PBS and incubating for 10 min at ambient temperature in Ca^{2+}-free PBS supplemented with 0.025% trypsin. Dissociated islet cells prepared from pre-diabetic or diabetic mice were stained for CD45 to identify infiltrating lymphocytes, followed by washing, immediate fixation, and permeabilization (4% paraformaldehyde, 0.1% saponin/PBS, 30 min). After removing paraformaldehyde by washing in 0.1% saponin/1% BSA/PBS, islet cells were stained intracytoplasmically for 30 min with antibodies to insulin (guinea pig; Dako), pancreatic polypeptide (rabbit; LabVision, Fremont, CA), and two mouse IgG1 monoclonal antibodies specific for glucagon (K79bB10; Sigma) and somatostatin (SOM018; antibody core facility, Beta Cell Biology Consortium, Antibody Care Unit, Målov, Denmark). Simultaneous staining using both mouse IgG1 antibodies required Invitrogen's Zenon (pre)labeling technology (Pacific Blue, AlexaFluor488). Highly cross-absorbed, second-step polyclonal antibodies, anti–guinea pig Cy5, and anti-rabbit PE were from Jackson ImmunoResearch. After the final wash in 1% BSA/saponin, cells were postfixed in 1% paraformaldehyde and acquired using a CyAn ADP flow cytometer (Beckman-Coulter) using Summit version 4.3 software. Electronic gating was set to include viable cells based on forward light scatter versus side light scatter. The doublet-exclusion gating setup diminished nondissociated islet cell couplets based on pulse width versus total signal area (linear scale) by ~20-fold, yet they did not significantly alter the relative endocrine cell frequencies and the calculated cell ratios (supplemental Fig. 1, available in an online appendix at http://diabetes.diabetesjournals.org/cgi/content/full/db08-0616/DC1).

Immunofluorescence and immunohistochemistry. Consecutive formalin-fixed paraffin-embedded sections (6 μm) were hematoxylin and eosin stained or subjected to immunostaining. Briefly, after blocking with 2% BSA/1% donkey serum and blocking reagent (M.O.M. kit; Vector, Burlingame, CA), primary antibodies (same as described for flow cytometry above, except for the rabbit–anti-glucagon antibody [Dako]) were reacted overnight at 4°C, washed three times (5 min, PBS 0.1% BSA, 0.1% Tween 20), and then stained for 1 h using anti–guinea pig Cy3 (Jackson ImmunoResearch), anti-rabbit AlexaFluor488, and anti-mouse AlexaFluor647 (Invitrogen) polyclonal antibodies and counterstained with 4′6-diamidino-2-phenylindole (5 min). Fluorescence analysis was performed on a Zeiss LSM 510 confocal microscope using Zeiss LSM 510 Meta software (Carl Zeiss Microimaging, Thornwood, NY).

For immunohistochemistry, tissue was weighed, spread on filter paper, and immediately fixed in 10% formalin. Formalin-fixed paraffin-embedded sections were antibody stained for insulin (Dako) or glucagon (Sigma) as above and then reacted with diaminobenzidine staining kits (Vector Labs) and counter stained with hematoxylin and eosin. Sections had an average tissue area of 72 mm^2 (63 mm^2 for diabetic pancreata), and the cumulative tissue area was scored from 3–7 sections spatially separated by 200 μm (surface-area range studied: 154–648 mm^2 per pancreas). Slides were scanned and analyzed using a Scanscope CS system with ImageScope software (Aperio Technologies, Vista, CA). The insulin-positive β-cell– and glucagon-positive α-cell mass was calculated from the sections by fractional cell staining over total pancreas area for insulin- and glucagon-positive cells, respectively.

Stimulated glucagon secretion and quantification. Glucagon secretory responses to 2-deoxy-glucose (2-DG) were carried out as previously described (19). Briefly, 200 μl retro-orbital blood was collected from newly diabetic and age- and sex-matched naïve nondiabetic Rip-CD80$^+$GP$^+$ mice. After fasting the animals overnight, two additional blood samples were taken from each mouse before and, as a terminal procedure, 15 min after injecting the glucose analog 2-DG (500 mg/kg i.p.). Serum was collected and stored frozen at −70°C. Serum glucagon concentrations were determined using radioimmunoassay (Millipore, St. Charles, MO).

Statistical analysis. An independent Student's *t* test (one-tailed) was chosen to test the significance of deviations between data sets (endocrine cell numbers or ratios). All data were displayed as the means ± SE.

RESULTS

Although hormone-producing cells can be visualized by multicolor immunofluorescence (Fig. 1*A*), we sought to more objectively quantify isolated pancreatic islets' endocrine cell frequencies using intracytoplasmic, multicolor flow cytometry to simultaneously detect insulin-, glucagon-, somatostatin-, and in some cases pancreatic polypeptide–positive cells. Figure 1*B* and supplemental Fig. 1 illustrate the detailed multiparameter flow cytometry results of an islet cell suspension from naïve C57BL/6 mice. We observed no overlap between the different endocrine cell subsets, thus confirming mature endocrine cells' known lineage separation (i.e., each endocrine cell produces only one hormone). Artifactual dual-hormone staining resulting from heterogeneous endocrine cell couplets was eliminated by routinely applying doublet-exclusion gating strategies. We validated the flow cytometry technique by comparing adult C57BL/6 mouse endocrine cell subset frequencies determined using flow cytometry and immunofluorescence and obtained quite concordant results (Fig. 1*C*) that were also consistent with published data (20,21).

Next, using our β-cell antigen-specific EAD model (17), we tracked insulin-positive endocrine cell optical properties by flow cytometry, and we tracked their abundance by immunofluorescence or immunohistochemistry, flow cytometry, and qRT-PCR during the islet inflammatory process leading to diabetes. Flow cytometry revealed markedly altered optical and staining properties displayed by the insulin-staining β-cells remaining at diabetes onset (Fig. 2). Of particular note, some but not all β-cells remaining in diabetic mice are larger (or hypertrophic) compared with naïve mouse β-cells (Fig. 2*A*). In addition, virtually all diabetic mouse β-cells displayed reduced granularity (i.e., decreased side light scatter) (Fig. 2*B*), strongly suggesting a diminished cytoplasmic insulin granule content (degranulation). Coincident with these optical changes, we found that diabetic mouse β-cells' insulin staining intensity was less than that observed from naïve mouse β-cells. To quantify this decline in individual β-cell insulin content, we found that nondiabetic mouse β-cell insulin staining was ~30-fold greater than nonspecific cellular fluorescence, whereas recently diabetic mice had only ~10-fold higher insulin-positive staining over background (Fig. 2*C*). This phenomenon was previously suspected (22) but could not be objectively quantified using conventional immunofluorescence.

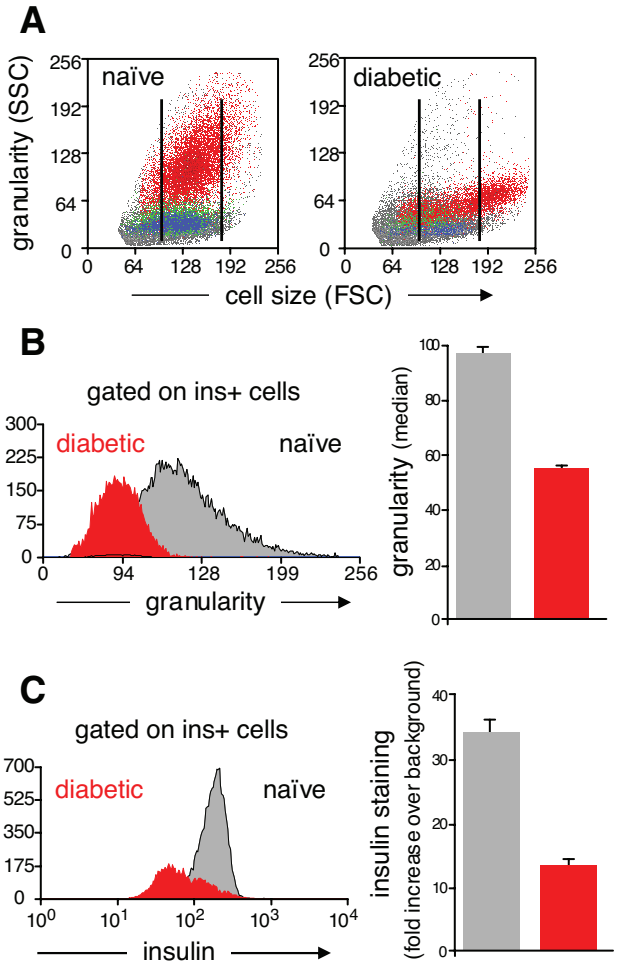

FIG. 2. Diabetic mouse β-cell optical changes by flow cytometry. *A*: Light scatter properties (cell size, forward light scatter [FSC]; and granularity, side light scatter [SSC]) of dissociated islet cells (red, β-cells; green, α-cells; blue, δ-cells) from naïve and diabetic mice are shown. β-Cell size distribution differs between naïve and diabetic mice. *B*: Granularity (SSC) properties of naïve (gray) and diabetic (red) islet cells gated on insulin-stained cells, displayed by histogram overlay, and quantified by median side light scatter signal. *C*: Insulin-staining brightness (median fluorescence intensity) of naïve (gray) and diabetic (red) β-cells is compared and plotted by histogram overlay and fold increase over non–insulin-positive islet cells (background staining). ins+, insulin-positive. (A high-quality digital representation of this figure is available in the online issue.)

We also examined the fate of other endocrine cell subsets in both healthy naïve mice (Fig. 3*A–C*) and in mice with recent-onset diabetes (Fig. 3*D–F*). As expected, healthy naïve Rip-CD80$^+$GP$^+$ bitransgenic mice closely resembled C57BL/6 mice, both by immunofluorescence (Fig. 3*A* and *B*) and by flow cytometry (Fig. 3*C*). In contrast, heavily immune cell-infiltrated islets from diabetic Rip-CD80$^+$GP$^+$ mice revealed a distorted picture (Fig. 3*E–F*). Because the islets were infiltrated with mononuclear immune cells, the endocrine cells were reduced in number and scattered (Fig. 3*E*). We were surprised to observe, however, that the residual endocrine cell frequency (suggested by immunofluorescence and quantified by flow cytometry) (Fig. 3*F*) was not consistent with a selective insulin-positive β-cell loss. Rather, glucagon-positive α-cell numbers decreased commensurate with the

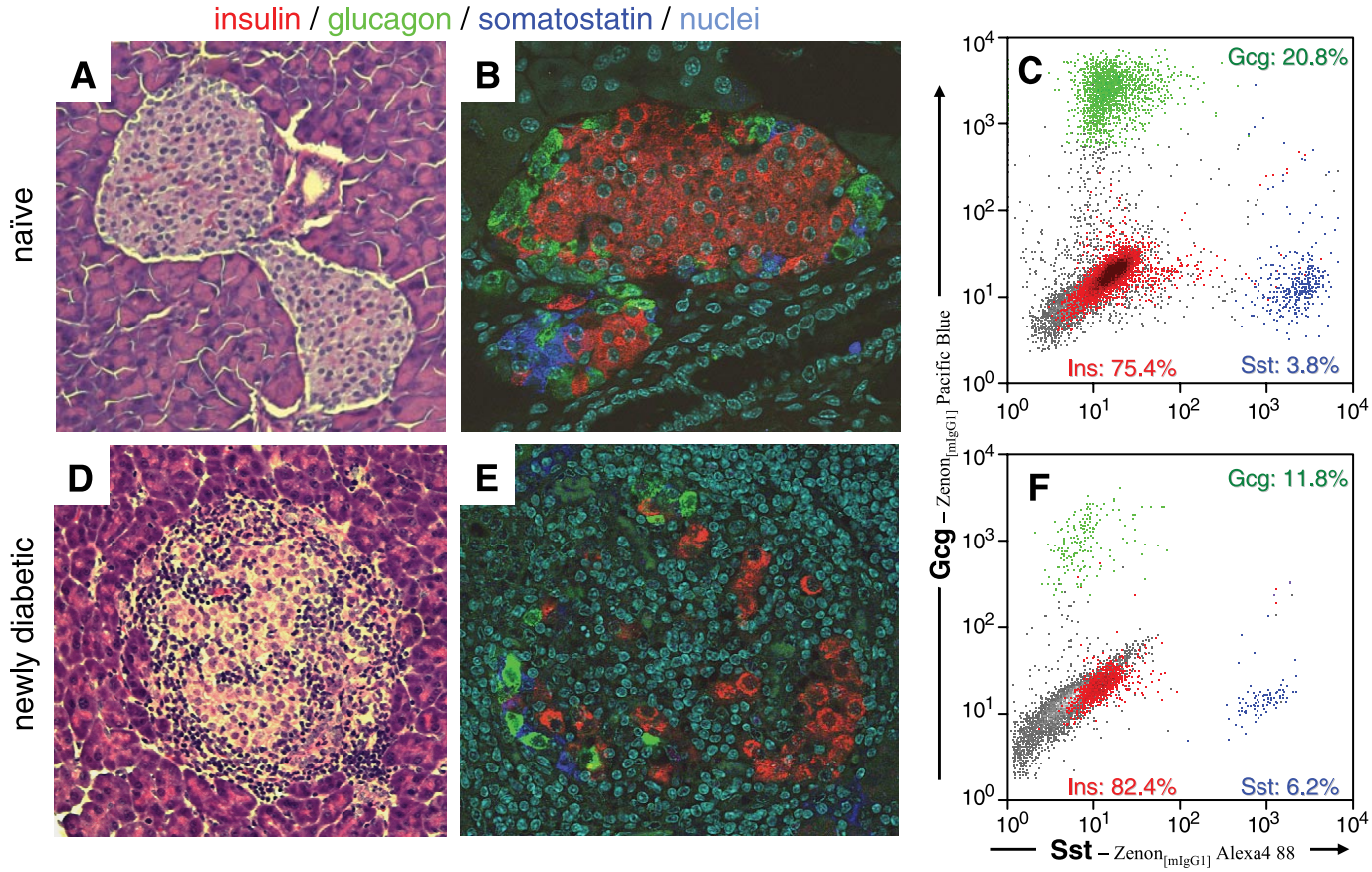

FIG. 3. Comparative analysis of naïve and diabetic pancreatic islets by immunofluorescence and flow cytometry. Islets from naïve (*A–C*) and recently diabetic mice (*D–F*) were examined by tissue sectioning and hematoxylin and eosin staining (magnification ×200) (*A* and *D*) and three-color immunofluorescence (magnification ×400) (*B* and *E*). Typical islets are shown (*A–B*, *D–E*). In addition, islets from an individual naïve or diabetic mouse were purified, dissociated, and analyzed by flow cytometry (*C* and *F*). Flow cytometry results were normalized as in Fig. 1. *F*: The drastically increased unstained cells (events shown in gray) represent cells within the islets that did not stain for any of the three islet hormones, insulin, glucagon, or somatostatin, nor for the hematopoetic cell marker CD45, which had been excluded by electronic gating. Thus, these cells represent islet cell components relatively enriched in inflamed, severe, endocrine cell–depleted islets. Note that the relative frequency of insulin-positive cells did not decrease compared with glucagon-positive cells and, in this case, only marginally compared with somatostatin-positive cells. Gcg, glucagon; Sst, somatostatin. (A high-quality digital representation of this figure is available in the online issue.)

insulin-positive β-cell numbers. Indeed, whereas we expected to find the insulin-positive–to–glucagon-positive cell ratio substantially reduced in diabetic mice, the cell ratio calculated using the flow cytometry technique often increased, suggesting that glucagon-positive cell numbers fell even more than insulin-positive cell numbers.

Previous reports using immunohistochemistry to study the pancreas in rodents undergoing acute β-cell injury, e.g., after streptozotocin administration (23,24) or spontaneous autoimmune islet destruction (25–27), have suggested that residual pancreatic endocrine cells in diabetic animals are comprised primarily of glucagon-positive and/or somatostatin-positive cells. All such studies, however, have evaluated mice with near "end stage" diabetes, whereas the EAD model allows us to better control both the initiation and the kinetics of the β-cell killing. We used several independent techniques to comprehensively examine pancreatic endocrine cell composition in EAD mice with recent-onset diabetes. As shown in Fig. 4*A* and *B*, we determined insulin-positive–to–glucagon-positive cell ratios from naïve and diabetic mice by flow cytometry and by immunofluorescence. Dissociated islet cells isolated from healthy control animals then analyzed by flow cytometry had a ratio of 4.9 ($n = 9$), which was comparable to immunofluorescence histology (4.7, $n = 3$). In contrast, islets analyzed from diabetic animals revealed a markedly increased ratio when analyzed by flow cytometry (9.8, $n = 11$) compared with immunofluorescence (4.2, $n = 9$).

Although flow cytometry determines relative frequencies of islet cell subsets with high fidelity, its translation into absolute cell numbers per pancreas has not been possible. Therefore, we used quantitative immunohistochemistry on multiple sections throughout the whole pancreas in recently diabetic mice to determine changes in absolute β- and α-cell numbers at diabetes onset. As shown in Fig. 4*C*, recently diabetic Rip-CD80$^+$GP$^+$ bitransgenic mice revealed the expected β-cell loss (an approximate 76% decrease relative to the healthy control animals) but also a corresponding depletion of α-cells (73% decrease) (Fig. 4*D*); each change is statistically significant ($P < 0.001$). To test whether the observed α-cell loss was unique to our EAD model, we extended our study to include the NOD mouse. As shown in Fig. 4*C* and *D*, a comparable pattern was observed in pancreas sections from newly diabetic NOD mice (age of diabetes onset: 18.2 ± 1.8 weeks) when compared with similarly aged female NOD-Rag1 null mice (13.4 weeks). Notably, however, nondiabetic NOD mice had about half as many total β- and α-cells compared with the Rip-CD80$^+$GP$^+$ bitransgenic mice, and at diabetes onset, the NOD mice were more severely β-cell–depleted than EAD mice. That is, diabetic NOD mice had lost 90% of their β-cells (Fig. 4).

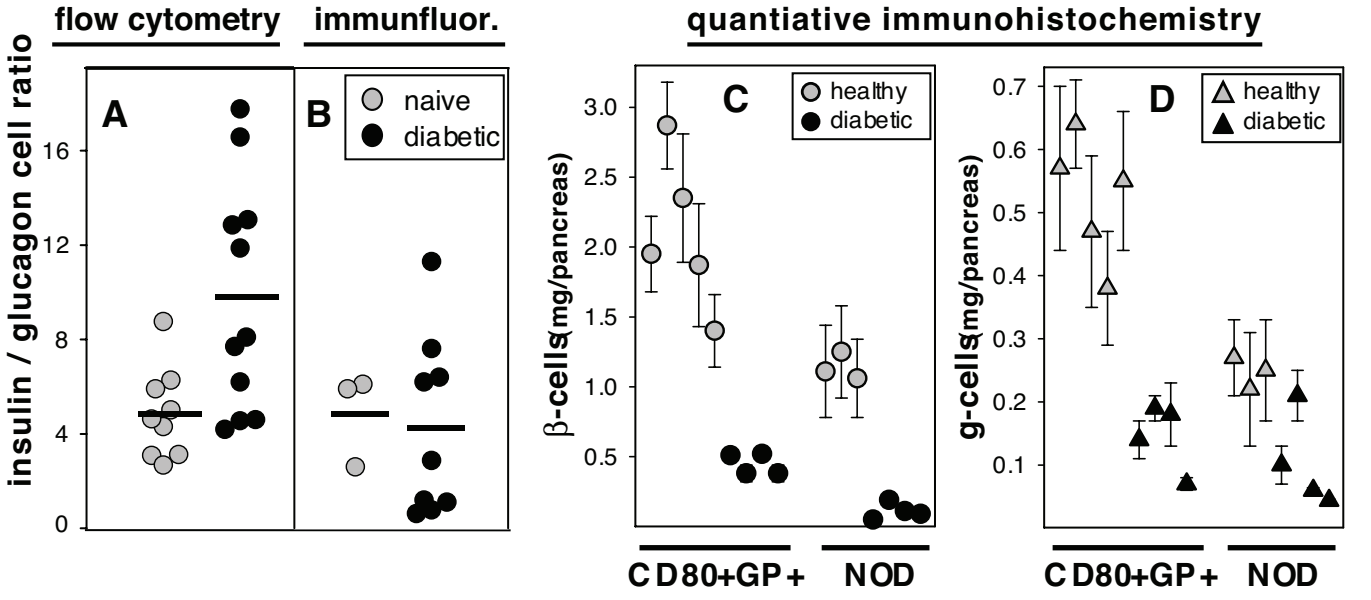

FIG. 4. Endocrine cell quantification using flow cytometry and quantitative immunohistochemistry. Pancreata from naïve (gray symbols) and diabetic EAD mice (black symbols) were examined by multicolor flow cytometry (*A*) and immunofluorescence microscopy (*B*). Insulin-positive–to–glucagon-positive cell ratios were plotted, with each symbol representing an individual mouse. Horizontal bars indicate the arithmetic means for groups of mice; they were 4.9 and 9.8, respectively, for naïve and diabetic mice in panel *A* and 4.9 and 4.2, respectively, for panel *B*. Note that purified, handpicked islets were used for flow cytometry in *A*, whereas in *B*, all microscopically detectable insulin- or glucagon-stained cells were scored. *C*: β-Cell mass. *D*: α-Cell mass from naïve ($n = 5$) and diabetic ($n = 4$) EAD mice (*C* and *D*, *left side*) and groups of age-matched NOD-Rag1 null ($n = 3$) and diabetic NOD mice ($n = 4$) (*C* and *D*, *right side*) were determined by image analysis of insulin or glucagon immunohistochemistry. Each symbol represents the cumulative fractional cell mass per pancreas, and the error bars indicate the SEM of 3–7 individual sections per pancreas. Differences in diabetic and naïve control pancreata were all found to be statistically significant ($P < 0.001$, except for glucagon-positive cell loss in NOD mice [$P = 0.026$]). immunofluor., immunofluorescence.

These changes were highly statistically significant ($P < 0.001$). In the NOD mice, the α-cell depletion was less severe (58% or 2.4-fold) (Fig. 4*D*) and with $P = 0.026$ did not reach the same high statistical significance we observed in the EAD model. The greater β-cell loss compared with α-cell loss in diabetic NOD mice resulted in a moderately reduced insulin-positive–to–glucagon-positive cell ratio (1.34 ± 0.28, $n = 7$). For instance, Fig. 5 shows representative flow cytometry analyses from islet cells taken from diabetic (*middle panels*), nondiabetic (*top panels*), and NOD-SCID mice (*lower panels*). We conclude that both Rip-CD80$^+$GP$^+$ and NOD mice with severe insulin deficiency caused by T-cell–mediated β-cell killing also lose many α-cells, such that shortly after diabetes onset, the insulin-positive–to–glucagon-positive cell ratio is actually maintained or increased in many Rip-CD80$^+$GP$^+$ mice and only moderately reduced in NOD mice, despite a more profound β-cell loss in the latter strain.

Next, we asked whether this discrepancy could be attributed, in part, to differential endocrine cell subset distribution in large islets compared with smaller, sub–islet-sized endocrine clusters that are scattered throughout the pancreas. In the EAD model, during the autoimmune process, such small endocrine cell clusters are characteristically surrounded by a marked leukocytic infiltration. We "scored" endocrine cells using immunofluorescence microscopy (Fig. 6*A*) and arbitrarily grouped the results into those from small clusters (<30 endocrine cells per islet cross section, which calculates to an islet diameter as small as 50–70 μm, depending on the level of lymphocytic infiltration) and larger islets (≥30 endocrine cells per islet). Although no difference in the insulin-positive–to–glucagon-positive cell ratio was found in naïve healthy pancreata from either C57BL/6 or Rip-CD80$^+$GP$^+$ strains (Fig. 6*A*), pancreata from diabetic mice displayed a substantial distortion; larger islets displayed an increased insulin-positive–to–glucagon-positive cell ratio, whereas small clusters had a decreased ratio (Fig. 6*A*). A quadratic regression analysis comparing the endocrine cell ratio to islet-size relationship is illustrated in more detail in supplemental Fig. 2.

We reasoned that the discrepant results shown in Fig. 4*A* and *B* (i.e., greater insulin-positive–to–glucagon-positive dispersed diabetic islet cell ratio by flow cytometry) may have been caused by failure to collect and analyze the exceedingly small, sub–islet-sized endocrine cell clusters from pancreas digests for flow cytometry. To test that possibility, we used flow cytometry to calculate the ratio from conventionally purified islets and from an islet-depleted, viable pancreas digest (Fig. 6*B–G*). Although the ratio was comparable in naïve mice (Fig. 6*B–D*), diabetic mice demonstrated a marked difference, with purified islets displaying a higher ratio, whereas islet-depleted pancreas digests had a decreased ratio (Fig. 6*E–G*). qRT-PCR used to compare the insulin to glucagon mRNA from purified islets and islet-depleted tissue confirmed that the purified islets lost at least as much glucagon compared with insulin mRNA (supplemental Fig. 3). The lower abundance of endocrine cells present in islet-depleted pancreas digests suggests that the overall insulin-positive–to–glucagon-positive cell ratio decrease reflects a more precipitous (immune-mediated) β-cell loss outside the confines of traditionally recognized islets, rather than increasing α-cell number. For instance, as illustrated in supplemental Fig. 4, we observed that single β-cells or small β-cell clusters were harder to find, were nearly always surrounded by inflammatory immune cells in diabetic animals, and, unlike in the healthy pancreas, often had glucagon-positive cells nearby.

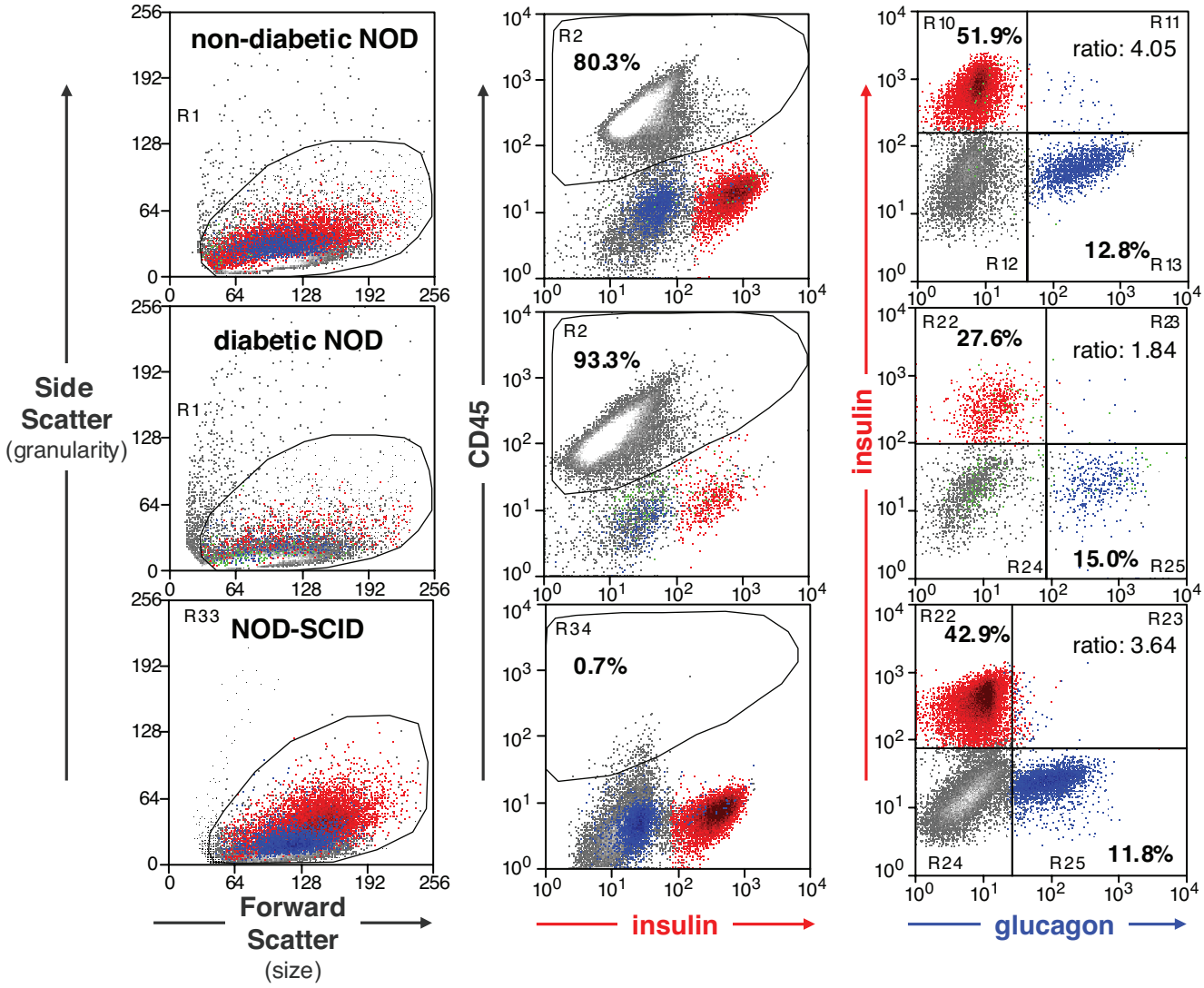

FIG. 5. Analysis of purified NOD islet cell suspensions by flow cytometry. Results from 23-week-old nondiabetic (*upper panels*), 15-week-old newly diabetic female NOD (*middle panels*), and 18-week-old NOD-SCID (*lower panels*) mice are shown. Gating strategy involved consecutive light scatter (*left column*), exclusion of CD45-positive lymphocytes (*center column*), doublet exclusion (not shown), and relative frequencies of insulin-positive β-cells versus glucagon-positive α-cells (*right column*). The β-cell–to–α-cell ratio of ~4 in both representative nondiabetic mice (average β-cell–to–α-cell ratio was 3.4 ± 0.5, n = 7, and 4.0 ± 0.2, n = 3, respectively, for nondiabetic NOD and NOD-SCID mice) dropped to 1.8 in the diabetic NOD mouse (average for this group: 1.3 ± 0.3, n = 7) due to a more profound loss in the β-cell compartment. Infiltrating CD45-positive lymphocytes were absent in NOD-SCID islets, but plenty were found in isolated islets of both NOD mice, being more abundant in the diabetic animal. Note the decreased β-cell granularity reflected by a low side scatter in all NOD mice shown, indicating possibly fewer or less-developed insulin granules in this mouse strain even in the absence of immune-mediated organ injury in NOD-SCID mice (*left column*, *lower panel*). Granularity seemed further reduced as the mice progressed toward autoimmune diabetes (*left column*, *top and middle panels*). (A high-quality digital representation of this figure is available in the online issue.)

Immunofluorescence microscopy of pancreata from mice with recent-onset EAD did not establish a consistent loss of β-cells over α-cells but, rather, revealed a broad range of relative cell abundances (supplemental Table 1). We therefore sought to examine individual mouse pancreata in greater detail. To this end we examined random pancreatic sections from naïve and diabetic EAD mice, previously used for endocrine cell quantification (Fig. 4*B* and *C*). In naïve mice, we found the expected β- and α-cell spatial orientation in islets and uniformly throughout the organ (Fig. 7*A–D*). In contrast, the diabetic mouse pancreas analysis displayed marked differences, with two distinct histopathological patterns occurring in the same organ. The first pattern was characterized by scarce, scattered insulin-positive cells within infiltrated islets, resulting in near parity of β- and α-cell numbers (Fig. 7*E–H*), which is a pattern consistent with an autoimmune process that selectively destroyed most β-cells but left α-cells unharmed. The second pattern revealed a similar abundance of insulin-staining cells in severely infiltrated islets along with dramatically reduced glucagon-stained α-cells (Fig. 7*I–L*), a finding not easily explained by a β-cell–specific deletion process. The two patterns were not randomly distributed within the pancreas, but one or the other pattern predominated in specific anatomical lobes (or lobules), where the vast majority of islets tended to show the same cell pattern.

Finally, we sought to address whether the observed α-cell loss might have a measurable functional correlate. We tested glucagon serum levels in both fed and fasted mice and in response to 2-DG–induced intracellular hypoglycemia. 2-DG was chosen over insulin-

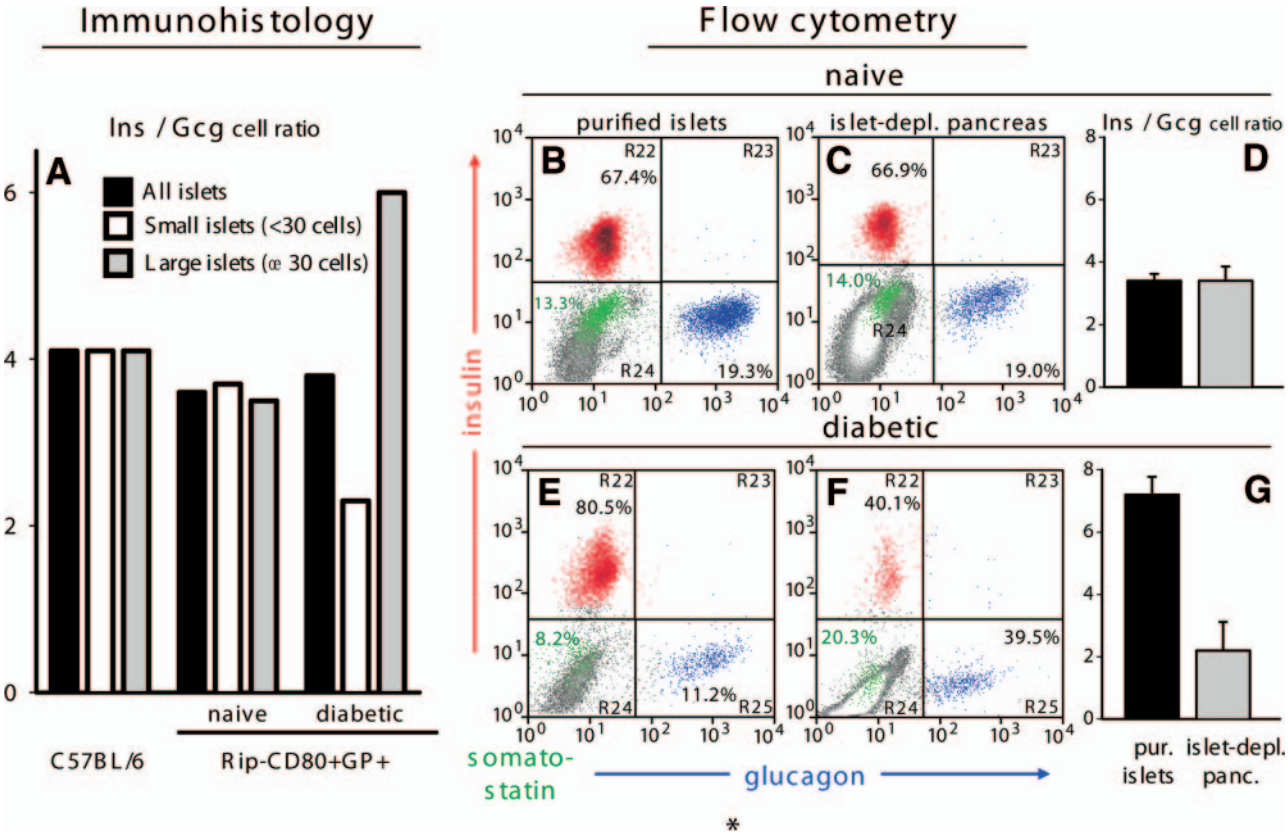

FIG. 6. Quantification of endocrine cells in large islets or sub–islet-sized endocrine clusters of. *A*: Relative abundance by immunofluorescence histology of β- and α-cells associated with islets or sub–islet-sized endocrine clusters in naïve and recently diabetic mice. Endocrine cells were counted from sections and subdivided in groups of small–endocrine cell clusters (<30 endocrine cells per cross section, □) or large islets (≥30 endocrine cells per cross section, ▨) and the sum of both (all islets, ■). The insulin-positive–to–glucagon-positive cell ratio of naïve C57BL/6 (n = 3) and naïve and diabetic Rip-CD80$^+$GP$^+$ mice (n = 3 and n = 5, respectively) was plotted for each islet size group. Insulin-, glucagon-, and somatostatin-positive cell frequencies were measured by flow cytometry in different pancreas compartments and from both naïve and recently diabetic mice. Purified islet cells (*B* and *E*) and viable, islet-depleted pancreatic tissue (*C* and *F*) were isolated from naïve (*upper panels*) and diabetic mice (*lower panels*). Representative flow cytometry plots and the calculated relative frequency of endocrine cell subsets are shown. *D* and *G*: The averages of insulin-positive–to–glucagon-positive cell ratios among islets and islet-depleted tissue (containing the small endocrine cell clusters) from healthy (n = 4) (*D*) and diabetic mice (n = 3) (*G*). depl., depleted; Gcg, glucagon; Ins, insulin; panc., pancreas. (A high-quality digital representation of this figure is available in the online issue.)

induced hypoglycemia because exogenous insulin can suppress α-cell glucagon secretion (28). Fed and overnight-fasted glucagon levels were virtually unchanged and indistinguishable in diabetic mice compared with naïve control mice (Fig. 8). Remarkably, 2-DG–stimulated glucagon secretion was significantly blunted in the diabetic mice (Fig. 8). 2-DG–induced glucagon response could not have been influenced by elevated blood glucose levels because the newly diabetic Rip-CD80$^+$GP$^+$ mice (fed glucose >20 mmol/l) were restored to normoglycemia after overnight fasting (mean blood glucose 8.5 mmol/l and consistently negative for fasting urine glucose) (Fig. 8), almost certainly reflecting substantial residual β-cell number at this early disease time point. We cannot prove that the α-cell loss we observed at autoimmune diabetes onset and the ~50% reduction of 2-DG–stimulated glucagon secretion are causally related or whether α-cell regulation of glucagon mRNA and protein synthesis could be a contributing factor. Further careful investigations including α-cell gene expression profiles and the application of more sensitive organ perfusion approaches will likely have to determine the exact cause of the glucagon pathophysiology frequently observed in autoimmune diabetes.

DISCUSSION

This study's initial objective was to assess pancreatic β-cell numbers and physiology during immune-mediated islet destruction by following the insulin-positive–to–glucagon-positive cell ratios and other parameters made possible by advanced flow cytometry techniques. We were surprised to observe that the relative frequency of the two endocrine subsets consistently pointed to an unexpected depletion of α-cells, along with the expected β-cell loss at diabetes onset. It is important to point out that because the flow technique lacks an internal reference standard, one cannot accurately determine the absolute number of α- or β-cells in the pancreas, only their relative proportion. We therefore turned to immunofluorescence microscopy and quantitative immunohistochemistry, supported by qRT-PCR, to provide additional, overlapping, and independent techniques. As discussed in our results, all studies supported our initial conclusion that while β-cells are being depleted during autoimmune diabetes, many α-cells also disappear.

Several lines of thought make it unlikely that nonspecific cell-mediated cytotoxicity (i.e., bystander injury) caused the observed non–insulin-positive islet cell (i.e., α-cell) depletion. First, the insulin promoter–controlled

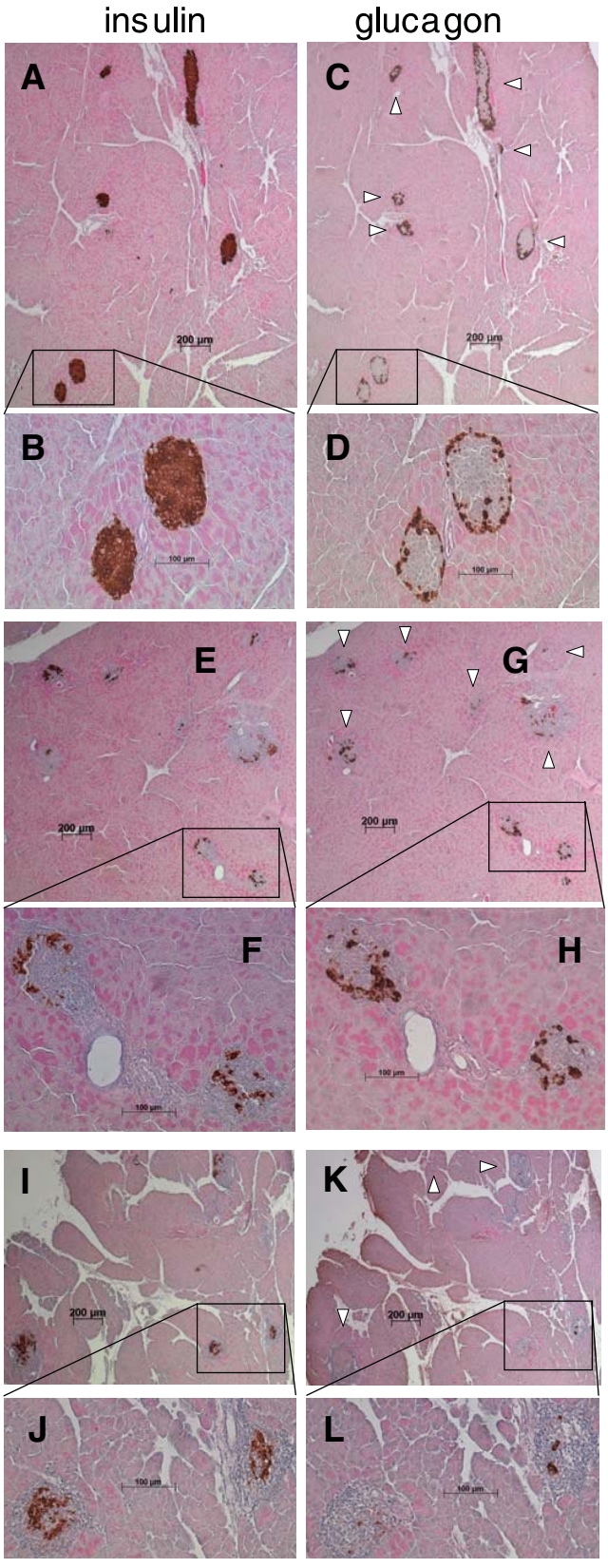

FIG. 7. Anatomical location within the pancreas determines the endocrine cell fate during diabetes development. Consecutive sections of one naïve (*A–D*) and one newly diabetic (*E–L*) Rip-CD80$^+$GP$^+$ mouse were analyzed for insulin staining (*left panels*) and glucagon staining (*right panels*) by immunohistochemistry. The naïve pancreas showed the expected abundance and spatial orientation of β- and α-cells in virtually all islets examined. Representative islets (*inset*) are shown with higher magnification (*B* and *D*). Groups of diabetic islets (arrowheads, depicted on glucagon-stained sections only) are shown from different lobes of the same pancreas (*E*, *G*, *I*, and *K*) and with higher magnification (*F*, *H*, *J*, and *L*). Note the uniform pattern of endocrine islet cell abundance in neighboring groups of islets. (A high-quality digital representation of this figure is available in the online issue.)

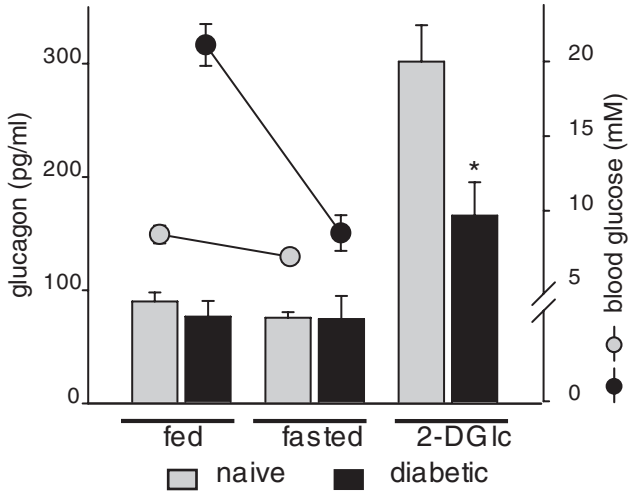

FIG. 8. Recently diabetic mice display lower secretory glucagon responses to 2-DG–induced intracellular (2-DG Ic) hypoglycemia. Blood glucose (circles) and serum glucagon levels from naïve (▨) and diabetic (■) Rip-CD80$^+$GP$^+$ mice were determined in random-fed mice (n = 7 and 4 for naïve and diabetic mice, respectively), in overnight-fasted mice (n = 16 and 8), and after 2-DG stimulation (n = 15 and 7). Serum glucagon levels are given as the means ± SE. *P < 0.003.

GP autoantigen is known to be specifically recognized by the adoptively transferred CTL (18,29), and transgenic CD80 molecules, which are essential for diabetes induction, are expressed homogenously on the transgenic mouse β-cell surface but not on other islet cell types (4). Whether all Rip-GP–transgenic β-cells express the GP transgene product is not known with certainty because detecting GP by immunofluorescence is hampered by mixed intracytoplasmic and nuclear expression patterns and by the limited availability of GP-specific antibodies. That LCM virus infection efficiently induces fulminant diabetes in Rip-GP mice (but never in wild-type controls) (30) strongly suggests that the vast majority of β-cells express the antigen leading to their immune-mediated destruction. In addition, the large proportion (30–70%) of the activated β-cell–monospecific TCR-transgenic CTLs found in EAD model mouse islets at diabetes onset argues in favor of a selective immune-targeting of the Rip-controlled dominant GP epitope in β-cells, and it does not support T-cell epitope spreading as the underlying autoimmune mechanism. Second, in past studies when we cotransplanted islets expressing the GP along with wild-type islets, only the GP-expressing β-cells were destroyed, despite an intense inflammatory infiltrate surrounding all the islets. In this environment nontransgenic islets were left microscopically intact and survived long-term (unpublished results), arguing against an effective inflammation-mediated bystander injury to α-cells. Finally, we have shown differential persistence of endocrine cells located in islets verses sub–islet-sized endocrine cell clusters, as well as very different endocrine cell ratios in anatomical parts of the same pancreas, with no discernible differences in the severity of immune cell infiltration. Taking all this data together, we favor a scenario where α-cell survival is homeostatically regulated in the context of deteriorating glycemia, possibly accompanied by regenerative pro-

cesses, which may affect distinct anatomical structures (e.g., pancreatic lobes) differently. It is also possible, however, that within typically identified islets, α-cell survival may be dependent upon a local β-cell–associated factor(s).

At diabetes onset, whereas insulin deficiency is axiomatic, abundant evidence suggests that pancreatic β-cells remain detectable for extended periods after disease diagnosis (31). It remains to be determined whether these β-cells persist after diabetes onset and/or are constantly regenerated. Most notably, an endocrine cell regenerative response has been reported to occur in several rodent models by mechanisms involving both β-cell proliferation (32,33) and/or neogenesis (34). Regenerative processes may be further stimulated in the presence of excess glucose (1) and by extensive organ injury (22). Moreover, neogenesis of insulin-producing cells by differentiation from non–β-cell precursors, such as ductal cells, could explain the abundant and scattered immune cell infiltrates we observe at diabetes onset, particularly infiltrates along ductal structures, often distant from any recognizable islet structure. Such regenerative neogenesis may partially or entirely recapitulate embryonic islet cell development (35) and differ among mouse strains. Thus, at present we can only speculate about the possibility that an accelerated β-cell regenerative process stimulated by severe immune-mediated β-cell killing and deteriorating glycemia causes a distorted distribution of those endocrine cells that are not insulin positive, especially α-cells. In this respect it is important to note that type 1 diabetic patients (36), and animals with autoimmune diabetes (37,38), are known to display aberrant glucagon secretory patterns. For instance, although fasting serum glucagon levels are usually normal in type 1 diabetes, they paradoxically can increase with overt hyperglycemia (39,40). Furthermore, many patients with type 1 diabetes fail to counterregulate hypoglycemia with adequate glucagon secretion (41,42), reminiscent of our results demonstrating that "intracellular" hypoglycemia-induced glucagon secretion is severely diminished in newly diabetic mice.

Our findings demonstrate that after autoimmune diabetes onset an endocrine cell's fate is dynamically regulated, responding to its micro- and macroenvironment. We argue that carefully unraveling the processes underlying autoimmune diabetes will illuminate pancreatic islet endocrine cell subsets' interdependence and may shed light on regenerative functions—including islet cell replication and neogenesis—that ultimately exhaust and fail, precipitating the onset of autoimmune diabetes.

ACKNOWLEDGMENTS

This research was supported by the Intramural Research Program of the National Institutes of Health, National Institute of Diabetes and Digestive and Kidney Diseases.

No potential conflicts of interest relevant to this article were reported.

The authors thank Alice Franks for mouse colony management, Eric Liu and Frank Leopardi for collagenase inflations of mouse pancreas, and Vipul Periwal and Arthur Sherman for regression analysis and critically reading the manuscript.

REFERENCES

1. Bonner-Weir S, Deery D, Leahy JL, Weir GC. Compensatory growth of pancreatic beta-cells in adult rats after short-term glucose infusion. Diabetes 1989;38:49–53
2. Sherry NA, Tsai EB, Herold KC. Natural history of beta-cell function in type 1 diabetes. Diabetes 2005;54(Suppl. 2):S32–S39
3. Valorani MG, Hawa MI, Buckley LR, Afeltra A, Cacciapaglia F, Pozzilli P. The natural history of insulin content in the pancreas of female and male non-obese diabetic mouse: implications for trials of diabetes prevention in humans. Diabetes Metab Res Rev 2004;20:394–398
4. Harlan DM, Barnett MA, Abe R, Pechhold K, Patterson NB, Gray GS, June CH. Very-low-dose streptozotocin induces diabetes in insulin promoter-mB7–1 transgenic mice. Diabetes 1995;44:816–823
5. Butler AE, Janson J, Soeller WC, Butler PC. Increased beta-cell apoptosis prevents adaptive increase in beta-cell mass in mouse model of type 2 diabetes: evidence for role of islet amyloid formation rather than direct action of amyloid. Diabetes 2003;52:2304–2314
6. Montanya E, Nacher V, Biarnes M, Soler J. Linear correlation between beta-cell mass and body weight throughout the lifespan in Lewis rats: role of beta-cell hyperplasia and hypertrophy. Diabetes 2000;49:1341–1346
7. Rabinovitch A, Russell T, Shienvold F, Noel J, Files N, Patel Y, Ingram M. Preparation of rat islet B-cell-enriched fractions by light-scatter flow cytometry. Diabetes 1982;31:939–943
8. Nielsen O, Larsen JK, Christensen IJ, Lernmark A. Flow sorting of mouse pancreatic B cells by forward and orthogonal light scattering. Cytometry 1982;3:177–181
9. Pipeleers DG, in't Veld PA, Van de WM, Maes E, Schuit FC, Gepts W. A new in vitro model for the study of pancreatic A and B cells. Endocrinology 1985;117:806–816
10. Halban PA, Powers SL, George KL, Bonner-Weir S. Spontaneous reassociation of dispersed adult rat pancreatic islet cells into aggregates with three-dimensional architecture typical of native islets. Diabetes 1987;36:783–790
11. Meyer K, Irminger JC, Moss LG, de Vargas LM, Oberholzer J, Bosco D, Morel P, Halban PA. Sorting human beta-cells consequent to targeted expression of green fluorescent protein. Diabetes 1998;47:1974–1977
12. Xu X, D'Hoker J, Stange G, Bonne S, De Leu N, Xiao X, Van De CM, Mellitzer G, Ling Z, Pipeleers D, Bouwens L, Scharfmann R, Gradwohl G, Heimberg H. Beta cells can be generated from endogenous progenitors in injured adult mouse pancreas. Cell 2008;132:197–207
13. Jayaraman S: A novel method for the detection of viable human pancreatic beta cells by flow cytometry using fluorophores that selectively detect labile zinc, mitochondrial membrane potential and protein thiols. Cytometry A. 2008;73:615–625
14. Chirgwin JM, Przybyla AE, Macdonald RJ, Rutter WJ. Isolation of biologically active ribonucleic acid from sources enriched in ribonuclease. Biochemistry 1979;18:5294–5299
15. Bonner-Weir S: Morphology of the endocrine pancreas. In *Principles and Practice of Endocrinology & Metabolism*. Becker KL, Ed. Lippincott Williams & Wilkins, 2001
16. Darwiche R, Chong MM, Santamaria P, Thomas HE, Kay TW. Fas is detectable on beta cells in accelerated, but not spontaneous, diabetes in nonobese diabetic mice. J Immunol 2003;170:6292–6297
17. Pechhold K, Karges W, Blum C, Boehm BO, Harlan DM. Beta cell-specific CD80 (B7-1) expression disrupts tissue protection from autoantigen-specific CTL-mediated diabetes. J Autoimmun 2003;20:1–13
18. Pircher H, Moskophidis D, Rohrer U, Burki K, Hengartner H, Zinkernagel RM. Viral escape by selection of cytotoxic T cell-resistant virus variants in vivo. Nature 1990;346:629–633
19. Ahren B, Taborsky GJ, Jr, Havel PJ. Differential impairment of glucagon responses to hypoglycemia, neuroglycopenia, arginine, and carbachol in alloxan-diabetic mice. Metabolism 2002;51:12–19
20. Brissova M, Fowler MJ, Nicholson WE, Chu A, Hirshberg B, Harlan DM, Powers AC. Assessment of human pancreatic islet architecture and composition by laser scanning confocal microscopy. J Histochem Cytochem 2005;53:1087–1097
21. Cabrera O, Berman DM, Kenyon NS, Ricordi C, Berggren PO, Caicedo A. The unique cytoarchitecture of human pancreatic islets has implications for islet cell function. Proc Natl Acad Sci U S A 2006;103:2334–2339
22. Sherry NA, Kushner JA, Glandt M, Kitamura T, Brillantes AM, Herold KC. Effects of autoimmunity and immune therapy on beta-cell turnover in type 1 diabetes. Diabetes 2006;55:3238–3245
23. Fernandes A, King LC, Guz Y, Stein R, Wright CV, Teitelman G. Differentiation of new insulin-producing cells is induced by injury in adult pancreatic islets. Endocrinology 1997;138:1750–1762
24. Li Z, Karlsson FA, Sandler S. Islet loss and alpha cell expansion in type 1 diabetes induced by multiple low-dose streptozotocin administration in mice. J Endocrinol 2000;165:93–99
25. Gomez Dumm CL, Console GM, Luna GC, Dardenne M, Goya RG. Quantitative immunohistochemical changes in the endocrine pancreas of nonobese diabetic (NOD) mice. Pancreas 1995;11:396–401
26. Pederson RA, Curtis SB, Chisholm CB, Gaba NR, Campos RV, Brown JC.

Insulin secretion and islet endocrine cell content at onset and during the early stages of diabetes in the BB rat: effect of the level of glycemic control. Can J Physiol Pharmacol 1991;69:1230–1236
27. Reddy S, Pathipati P, Bai Y, Robinson E, Ross JM. Histopathological changes in insulin, glucagon and somatostatin cells in the islets of NOD mice during cyclophosphamide-accelerated diabetes: a combined immunohistochemical and histochemical study. J Mol Histol 2005;36:289–300
28. Diamond MP, Hallarman L, Starick-Zych K, Jones TW, Connolly-Howard M, Tamborlane WV, Sherwin RS. Suppression of counterregulatory hormone response to hypoglycemia by insulin per se. J Clin Endocrinol Metab 1991;72:1388–1390
29. Ehl S, Hombach J, Aichele P, Hengartner H, Zinkernagel RM. Bystander activation of cytotoxic T cells: studies on the mechanism and evaluation of in vivo significance in a transgenic mouse model. J Exp Med 1997;185:1241–1251
30. Ohashi PS, Oehen S, Buerki K, Pircher H, Ohashi CT, Odermatt B, Malissen B, Zinkernagel RM, Hengartner H. Ablation of "tolerance" and induction of diabetes by virus infection in viral antigen transgenic mice. Cell 1991;65:305–317
31. Sosenko JM, Palmer JP, Greenbaum CJ, Mahon J, Cowie C, Krischer JP, Chase HP, White NH, Buckingham B, Herold KC, Cuthbertson D, Skyler JS. Patterns of metabolic progression to type 1 diabetes in the Diabetes Prevention Trial-Type 1. Diabetes Care 2006;29:643–649
32. Dor Y, Brown J, Martinez OI, Melton DA. Adult pancreatic beta-cells are formed by self-duplication rather than stem-cell differentiation. Nature 2004;429:41–46
33. Teta M, Rankin MM, Long SY, Stein GM, Kushner JA. Growth and regeneration of adult beta cells does not involve specialized progenitors. Dev Cell 2007;12:817–826
34. Bonner-Weir S, Toschi E, Inada A, Reitz P, Fonseca SY, Aye T, Sharma A. The pancreatic ductal epithelium serves as a potential pool of progenitor cells. Pediatr Diabetes 2004;5(Suppl. 2):16–22
35. Bonner-Weir S, Baxter LA, Schuppin GT, Smith FE. A second pathway for regeneration of adult exocrine and endocrine pancreas. A possible recapitulation of embryonic development. Diabetes 1993;42:1715–1720
36. Gerich JE, Langlois M, Noacco C, Karam JH, Forsham PH. Lack of glucagon response to hypoglycemia in diabetes: evidence for an intrinsic pancreatic alpha cell defect. Science 1973;182:171–173
37. Powell AM, Sherwin RS, Shulman GI. Impaired hormonal responses to hypoglycemia in spontaneously diabetic and recurrently hypoglycemic rats: reversibility and stimulus specificity of the deficits. J Clin Invest 1993;92:2667–2674
38. Jacob RJ, Dziura J, Morgen JP, Shulman GI, Sherwin RS. Time course of the defective alpha-cell response to hypoglycemia in diabetic BB rats. Metabolism 1996;45:1422–1426
39. Dobbs R, Sakurai H, Sasaki H, Faloona G, Valverde I, Baetens D, Orci L, Unger R. Glucagon: role in the hyperglycemia of diabetes mellitus. Science 1975;187:544–547
40. Greenbaum CJ, Prigeon RL, D'Alessio DA. Impaired beta-cell function, incretin effect, and glucagon suppression in patients with type 1 diabetes who have normal fasting glucose. Diabetes 2002;51:951–957
41. Bolli GB, Dimitriadis GD, Pehling GB, Baker BA, Haymond MW, Cryer PE, Gerich JE. Abnormal glucose counterregulation after subcutaneous insulin in insulin-dependent diabetes mellitus. N Engl J Med 1984;310:1706–1711
42. Hoffman RP, Arslanian S, Drash AL, Becker DJ. Impaired counterregulatory hormone responses to hypoglycemia in children and adolescents with new onset IDDM. J Pediatr Endocrinol 1994;7:235–244